applied sciences

Article

Laboratory Test and Constitutive Model for Quantifying the Anisotropic Swelling Behavior of Expansive Soils

Zhengnan Liu [1,2], Rui Zhang [1,3,4,*], Tian Lan [3,5], Yu Zhou [1] and Chao Huang [6]

1 School of Traffic and Transport Engineering, Changsha University of Science & Technology, Changsha 410114, China; lzn@csust.edu.cn (Z.L.); zy@stu.csust.edu.cn (Y.Z.)
2 Hunan Communications Research Institute Co., Ltd., Changsha 410015, China
3 National Key Laboratory of Green and Long-Life Road Engineering in Extreme Environment (Changsha), Changsha University of Science & Technology, Changsha 410114, China; lantian@hnust.edu.cn
4 Engineering Research Center of Catastrophic Prophylaxis and Treatment of Road & Traffic Safety of Ministry of Education, Changsha University of Science & Technology, Changsha 410114, China
5 School of Civil Engineering, Hunan University of Science and Technology, Xiangtan 411201, China
6 School of Civil Engineering, Central South University, Changsha 410075, China; huangchao-22@csu.edu.cn
* Correspondence: zr@csust.edu.cn

Abstract: Expansive soils exhibit directionally dependent swelling that traditional isotropic models fail to capture. This study investigates the anisotropic swelling characteristics of expansive soil with a medium swelling potential through the use of modified oedometric testing. Vertical swelling strains can reach up to 1.71 times that of the horizontal movements, confirming intrinsic anisotropy. A nonlinear elastic constitutive model incorporates vertical and horizontal elastic moduli with respect to matric suction to characterize anisotropy. Three elastic parameters were determined through the experiments, and predictive equations were developed to estimate the unsaturated moduli. The constitutive model and predictive techniques provide practical tools to better assess expansive soil pressures considering anisotropy, offering guidelines for utilization and design. The outcomes advance understanding of these soils' directionally dependent behavior and stress–strain–suction response.

Keywords: road engineering; constitutive model; swelling test; expansive soil; support structure

check for updates

Citation: Liu, Z.; Zhang, R.; Lan, T.; Zhou, Y.; Huang, C. Laboratory Test and Constitutive Model for Quantifying the Anisotropic Swelling Behavior of Expansive Soils. *Appl. Sci.* **2024**, *14*, 2255. https://doi.org/10.3390/app14062255

Academic Editors: Stefano Invernizzi and Marta Pérez Arlucea

Received: 10 January 2024
Revised: 21 February 2024
Accepted: 6 March 2024
Published: 7 March 2024

1. Introduction

Expansive soils are problematic soils that cause significant damage to infrastructure due to their shrinkage and swelling behavior influenced by changes in moisture content [1]. These soils contain high percentages of clay minerals such as smectite that have the capacity to absorb water into their crystalline structure [2]. Approximately 26 provinces in China contain expansive soils, posing major challenges for transportation and construction projects [3,4].

Expansive soils traditionally excavated from construction sites have been treated as construction and demolition waste and replaced with more engineered fill materials [5]. However, this practice is unsustainable and results in higher costs and environmental impacts from spoil disposal [6]. Recently, there has been a shift towards directly reusing expansive soils as pavement subgrades or engineered fill soils where feasible [7–9]. While this approach offers economic and sustainability benefits, it necessitates a deeper understanding of the mechanical behavior and earth pressure development characteristics of expansive soils, particularly under unsaturated conditions.

When expansive soils absorb moisture, either from rainfall infiltration or rising groundwater levels, they undergo significant volumetric expansion, commonly known as swelling. This process creates vertical swelling pressures that can damage shallow foundations and raise structures from their supporting soils. Additionally, it exerts lateral pressures against retaining walls, basements, and other structures, leading to structural cracking and failures if not adequately considered in their design [10]. Conversely, during dry periods, expansive soils shrink, contributing to differential settlement issues [11]. Therefore, there is a need to evaluate the swelling behavior of expansive soil and accurately estimate the earth pressure exerted by expansive soil against retaining structures, which is crucial for analyzing slope stability and designing retaining structures in expansive soil areas.

Previous research has primarily focused on characterizing the swelling behavior and stress–strain response of expansive soils through laboratory testing and constitutive modeling. Various empirical and mechanistic models have been developed to describe the volume change phenomena of expansive clays, capture hydromechanical coupling behavior, and enable numerical analysis and design applications [12–14]. For instance, Fredlund's model [15] is popular due to its simplicity, as it relates stress and strain conditions to net stress and matric suction states. The highlights are also focused on the acquisition and prediction of the elastic modulus [16,17]. However, many traditional models assume that expansive soils exhibit isotropic mechanical properties despite evidence that anisotropy is intrinsic to their fabric and swelling at the microstructural scale. The directional arrangement of clay minerals is known to influence the development and magnitude of swelling strains and pressures.

Recent studies have observed distinct anisotropic characteristics between vertical and horizontal swelling of intact expansive soil specimens [18–20]. From the microstructure analysis, flaky clay particles within expansive soils are inclined to orient horizontally after compaction; this preferred orientation phenomenon becomes more apparent with an increase in static pressure, consequently leading to significant differences in swelling behavior [21]. Several researchers have developed experimental methods for determining lateral swelling pressure by modifying traditional oedometer and hydraulic triaxial apparatus [22–26]. By using the modified oedometer apparatus, researchers have consistently found that measured lateral pressures exceed those in the vertical direction under inundation conditions. Additionally, the ratio of swelling pressure in the vertical and lateral directions varies with the surcharge, moisture, and density of the soil specimens [27,28]. This inherent material anisotropy is not fully considered in common isotropic constitutive formulations. Simplified elastic analysis of earth pressures acting on retaining walls may produce non-conservative estimates if true directional deformation behavior is not properly characterized.

The objective of this paper was to experimentally investigate the anisotropic swelling properties of problem expansive soil from southern China and develop a model that can reliably predict lateral earth pressures during wetting based on laboratory-calibrated parameters. A modified unsaturated consolidation testing method was devised to isolate vertical and horizontal swelling responses under controlled stress states. The test results were then used to determine the parameters for a proposed anisotropic elastic model featuring separate elastic moduli for the vertical and horizontal directions. Simple normalization techniques were applied to extend the model for use under varying degrees of saturation. Finally, the model was validated through a comparison of the estimated and measured lateral pressure development curves from consolidation testing. The proposed approach aims to advance practical analysis and design involving expansive soils considering directionally dependent swelling behavior.

2. Materials and Methods

2.1. Materials

The expansive soil used in this study was collected from a site (23°48′11″ N, 106°43′11″ E) along the Longlin–Baise Expressway in Baise, Guangxi Zhuang Autonomous Region, China. Index property tests were conducted to characterize the soil, and the results are shown in Table 1. Atterberg limits testing resulted in a liquid limit of 56.3% and a plastic limit of 21.4%, corresponding to a plasticity index of 34.9%. Particle size analysis revealed that the soil contained 47.9% clay-sized particles (<0.002 mm). X-ray diffraction analysis quantified the mineralogy as being 16.6% smectite, 22% illite, 24% kaolinite, and 1% chlorite.

Table 1. Index properties of the testing soil.

Description	w_L (%)	I_P	G_s	Sand (%)	Silt (%)	Clay (%)	USCS	MDUW (kN/m^3)	OMC (%)
Expansive soil	56.3	34.9	2.75	0	52.1	47.9	CH	17.2	17.9

Note: w_L: liquid limit; I_P: plasticity index; G_s: specific gravity; USCS: unified soil classification system; MDUW: maximum dry unit weight; and OMC: optimum moisture content.

Standard Proctor compaction tests were carried out following the requirement of American Society for Testing Materials (ASTM) [29] to determine the maximum dry unit weight (MDUW) and optimum moisture content (OMC) of the soil. Three specimens were compacted and tested at varying moisture levels, resulting in an MDUW of 17.2 kN/m^3 at an OMC of 17.9%. Free swell index tests indicated that the soil exhibited medium swelling potential according to Highway Engineering Geological Investigation (JTG C20-2011) [30].

2.2. Testing Method

A modified oedometer testing method was developed to capture the directionally dependent swelling behavior of the expansive soil. An automated unsaturated consolidation (UC) apparatus was constructed, incorporating controlled vertical load, lateral confinement, matric suction, and real-time displacement and pressure monitoring capabilities. The apparatus is illustrated in Figure 1.

The apparatus comprised several integrated subsystems within a rigid reaction frame. At the base, a consolidated drained pressure chamber housed a high air-entry value ceramic disk (HAEV disk), which was designed to apply and measure the air and water pressures independently. Digital pressure transducers integrated in the air and water pump with $\pm$1 kPa accuracy can regulate the air (0–500 kPa) and water (0–50 kPa) pressures, and a pressure transducer with $\pm$1 kPa accuracy was equipped on the loading rod connected to the reaction frame to control the vertical load (0–500 kPa) applied through the reaction frame and the vertical movement of the pressure chamber. Extensive drainage lines and outlet valves facilitated the saturation of the disk and equipment using a Mariotte bottle, as well as water delivery and bubble flushing. A pressure regulator maintained a low upward gradient (<50 kPa) to remove bubbles and ensure the full saturation of the HAEV disk. The saturated HAEV disk then acted as an air–water interface, transmitting pore–water stresses to the specimen above. During testing, the water pressure always remains constant at 40 kPa to accelerate the saturation of the HAEV disk and ensure an unobstructed water supply path. After the vertical load (σ_v), air pressure (u_a), and water pressure (u_w) were all applied in the pressure chamber, and the soil specimen was ready to be inundated under the given net normal stress ($\sigma_v - u_\mathrm{a}$) and matric suction ($u_a - u_w$). The linear variable displacement transducer (LVDT) for measuring axial strains was mounted on the loading rod and bracketed to the top of the pressure chamber, enabling precise measurements of the axial strains to a precision of 1×10^{-3} mm. Fine threaded rods connected the components and provided adjustability. Signals from the transducers interfaced with a data acquisition system, recording the pressures, vertical displacement, air pressures, and water pressures. Considering the fact that the permeability of expansive soil is extremely small, which results in quite a long period of time to achieve suction equilibrium, the frequency of the recording was set to 5 min intervals. The benchmark for the determination of suction equilibrium was also set as the changes in the readings for lateral pressure and vertical displacement were <1 kPa and 0.010 mm, respectively.

A significant innovation was the integration of a "retractable ring" device for the lateral confinement of the soil specimens during testing. As depicted in Figure 2, it consisted of a stainless steel ring with a 61.8 mm inner diameter and 30 mm height, housing a miniature pressure transducer (0–1000 kPa, $\pm$1 kPa accuracy), thin acrylic spacer, and a curved plate.

An adjustable tightening mechanism joined the halves of the ring, enabling it to close down in discrete steps to maintain the laterally confined state. After assembling, the retractable ring, which contained the loading piston, porous stone, specimen, and lateral miniature pressure transducer component, was positioned above the HAEV disk in the pressure chamber, as shown in Figure 1.

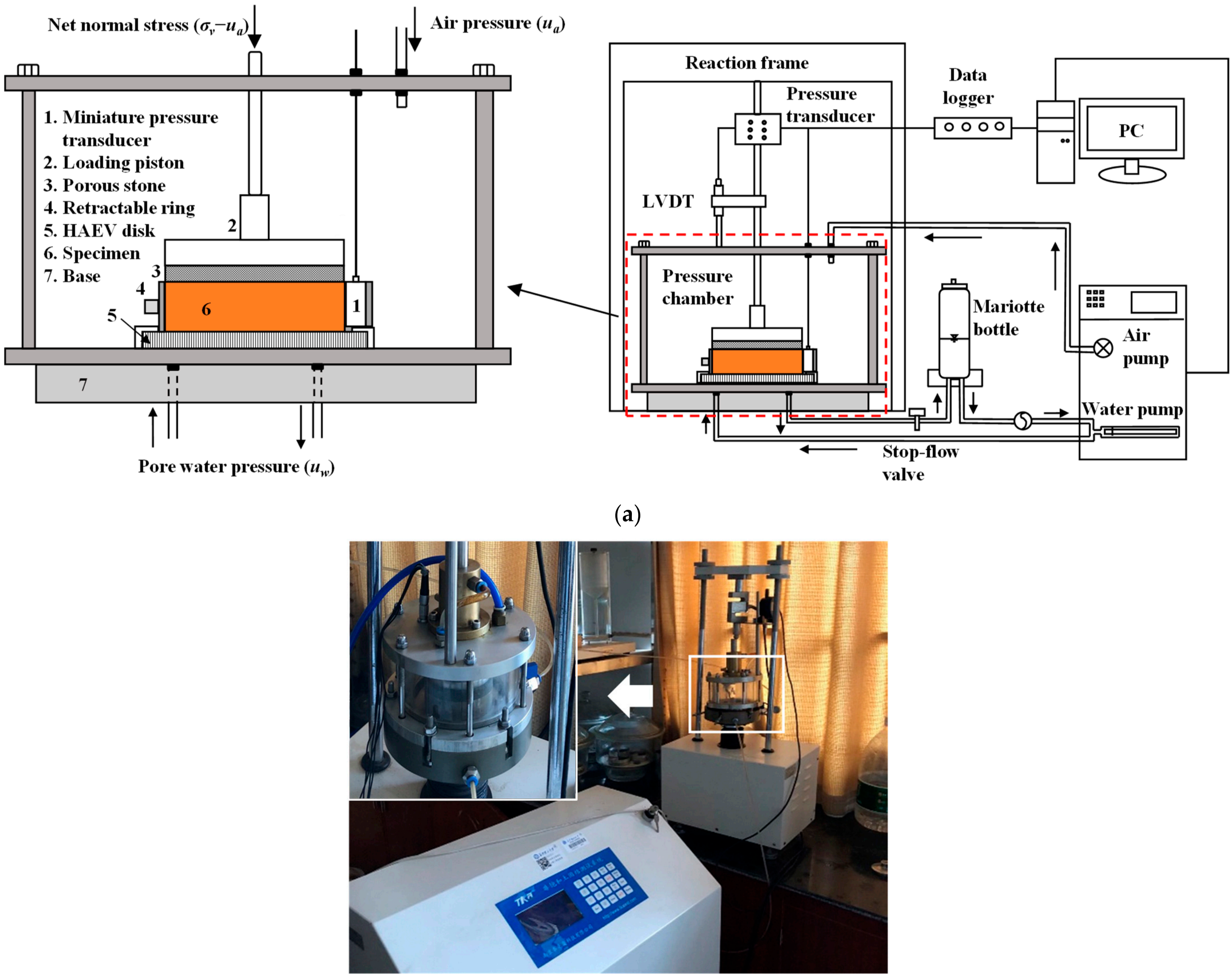

(**a**)

(**b**)

Figure 1. A (**a**) schematic view and (**b**) photo of the modified UC oedometer.

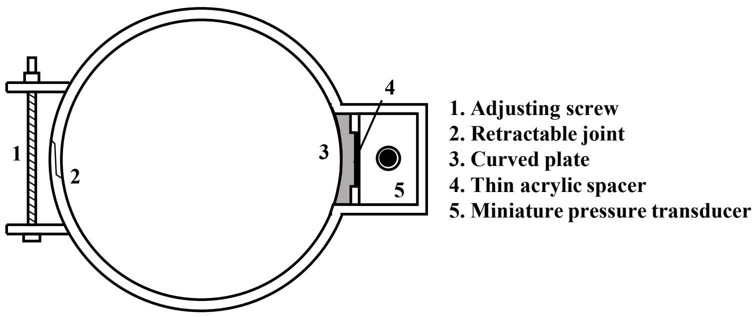

Figure 2. Schematic view of the retractable ring.

Extensive trials were conducted to calibrate the transducer readings and establish an optimal ring closure protocol. As depicted in Figure 3, the lateral pressure generated during the expansion of the specimen can be simulated by a controlled vertical load. Therefore, the calibration process started with a customized "T"-shaped loading frame, as shown in Figure 3a, which can be connected to the threaded loading head of the force gauge through a threaded hole in its upper part. The pressure would be gradually applied to the loading frame by the force gauge and transmitted through the curved plate and thin acrylic spacer to the miniature pressure transducer. The deformation is then monitored by two displacement gauges placed on both sides of the loading frame. Finally, the real-time readings of deformations and pressures are entered into the software interface (Ver 1.0) via displacement and pressure data loggers, respectively. It was observed that maintaining lateral stresses 2–3 kPa higher than the bulk stress state ensured reliable contact while minimizing boundary effects.

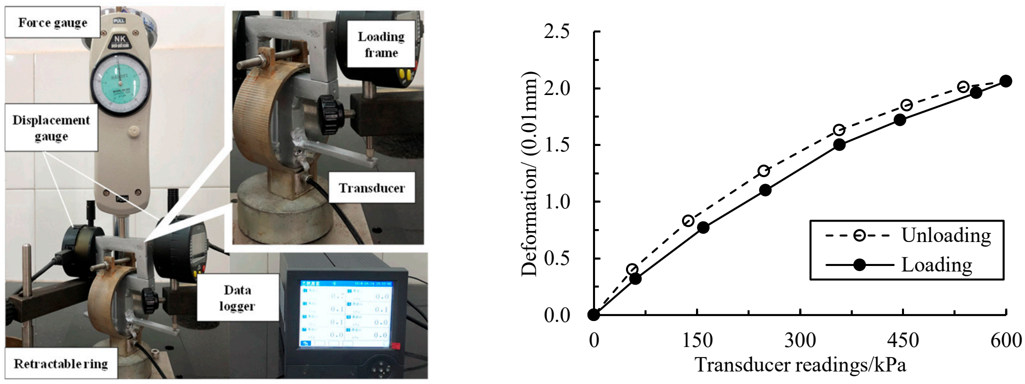

(**a**) (**b**)

Figure 3. Calibration of the retractable ring for the (**a**) process and (**b**) result.

In addition, as shown in Figure 3b, the maximum deformation obtained was 0.021 mm when the miniature pressure transducer reached the full scale of 600 kPa for the force gauge. Based on a specimen diameter of 61.8 mm, it can be calculated that the maximum radial strain is 0.032%, which is less than the requirement of the ASTM standard [31], which states that the maximum radial change in the ring should not be greater than the original diameter of 0.04% to achieve the K_0 condition. In addition, the influence of air pressure on the miniature pressure transducer was also considered. In the subsequent laboratory tests, the maximum value of the applied matric suction was set to 200 kPa; therefore, in the calibration process, the water pressure applied by the pump was always kept constant at 40 kPa, and the air pressure applied by the air pump ranged from 40 to 240 kPa to ensure that the formation of matric suction was in the range of 0–200 kPa. The results show that the readings of the miniature pressure transducer remained unchanged whether the air pressure was reduced from 240 kPa to 0 or increased from 0 to 240 kPa, which indicates that the effect of air pressure on the miniature pressure transducer in this study could be negligible.

Considering the disturbance and loss of moisture content during the transportation of the soil samples retrieved from the field, the specimens prepared in this way can no longer reflect the actual situation in the field. Therefore, remodeled soil samples were used in this study, and the pre-specimens were prepared in the manner of layered static compaction to approximate the layering phenomenon produced via the deposition of the original samples in the field. Specimen preparation involved drying, grinding, and sieving before compacting the samples under predetermined conditions. The expansive soil samples from the field were first dried in the oven at 105 °C, then ground to powder and passed through a sieve with a diameter of 2 mm. Subsequently, the samples were stored in a sealed plastic bag in the shade for at least 24 h. In addition, the expansive soils should be passed through the 2 mm sieve once more before specimen preparation since expansive soil easily clots after being mixed with distilled water.

The specimens were all prepared at an initial moisture content of 18.0% and a dry unit weight of 16.0 kN/m^3. Specimen homogenization entailed the static compaction of the prepared wet soil within a custom cube mold at each 10 mm layer. The compacted "pre-specimens" were extruded and vertically cut or rotated 90° prior to sampling for oedometer vertical swelling (OVS) or horizontal swelling (OHS) tests, respectively. As depicted in Figure 4, the modified preparation approach orientates clay mineral flakes differently to reflect field conditions.

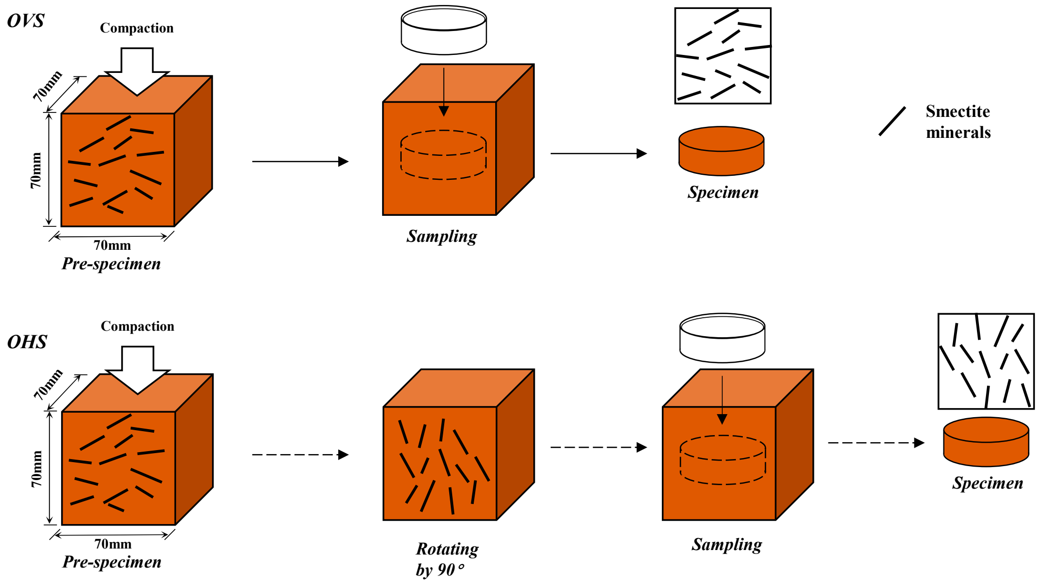

Figure 4. Schematic view of specimen preparation.

For the OHS tests, the pre-specimens were initially rotated 90° prior to coring. This modification oriented the platy clay structure differently to induce intrinsic anisotropy. The extracted specimens were then carefully positioned within the retractable ring for confinement during testing. Trimming and greasing of sample surfaces were carried out to minimize the effects of side friction.

A consistent test procedure was followed for all series under varying net normal stress conditions (Table 2). The initial matric suction of the specimens was measured as 500 kPa using the filter paper method before being gradually reduced in staged equilibrium steps. Vertical swelling displacements, lateral confining pressures, and equilibrium times were recorded, with pressure transducers monitoring net stresses.

Table 2. Summary of testing program conditions.

Type	Test ID	Dry Unit Weight (kN/m^3)	Moisture Content (%)	Net Normal Stress $\sigma_v - u_a$ (kPa)	Matric Suction $u_a - u_w$ (kPa)
OVS	OVS-0	16.0	18.0	0	200→100→50→20→10→5→0
	OVS-12.5			12.5	
	OVS-25			25	
	OVS-50			50	
	OVS-100			100	
OHS	OHS-0			0	
	OHS-12.5			12.5	
	OHS-25			25	
	OHS-50			50	
	OHS-100			100	

Each test series was conducted under constant net normal stress and followed the same decreasing matric suction path. For instance, OHS-12.5 denoted an OHS test series conducted with a net normal stress of 12.5 kPa, and 50→20 indicated that the controlled matric suction decreased from 50 kPa to 20 kPa. Furthermore, the compressed vertical strain of the specimen manifested once a certain net normal stress was applied, leading to the complete alteration of the initial volume and dry unit weight of the tested specimen. Therefore, the matric suction level of 500 kPa was not included, and the matric suction was initiated at 200 kPa.

Upon the completion of swelling under a given suction, the stresses were adjusted to maintain net stress while further lowering suction. The tests were terminated once specimens were fully saturated. This testing program generated a robust anisotropic stress–strain–suction dataset for characterizing soil behavior and developing constitutive models.

3. Experimental Results

The testing program produced a comprehensive dataset that characterizes the anisotropic swelling behavior of the expansive soil under varying stress conditions. Here, we present the key findings from the analysis of vertical swelling strain and lateral pressure responses measured across a range of controlled suction reductions.

Figure 5a illustrates the variations in the vertical swelling strain with matric suction reduction observed across all net normal stress conditions for the OVS and OHS test series. Several consistent trends were observed. Firstly, the swelling strains increased with decreasing suction as the soil moisture content rose for both test orientations. This behavior is consistent with the typical mechanisms of expansive soils gaining volume as water enters the diffused double layer of smectite clay plates.

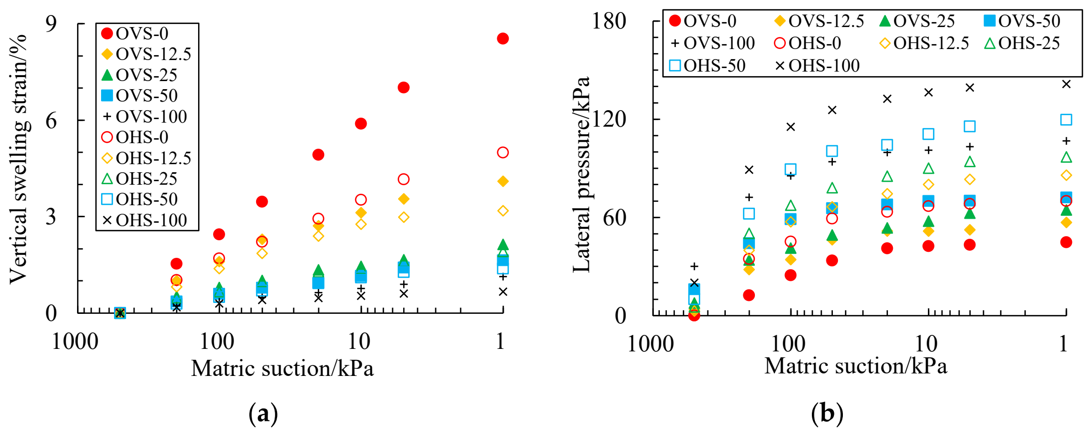

Figure 5. Variation in the (**a**) vertical swelling strain and (**b**) lateral pressure under different net normal stresses with matric suction.

Secondly, the strains in the vertical direction were significantly larger compared to the horizontal direction. At full saturation under zero net stress, the maximum vertical swell measured 8.54% in OVS, whereas only 4.99% horizontal swell occurred in the OHS tests. The vertical swelling strain in OVS was about 1.71 times that in OHS. This confirms the presence of intrinsic anisotropy, where clays expand more readily out of the plane of their layered structure due to the influence of depositional packing and consolidation stresses.

Thirdly, higher net normal stresses resulted in reduced vertical swell strains as confinement restricted volume changes. However, strains progressively increased with desaturation across all stress conditions, indicating a complex interaction between the applied stresses and changing suction states.

Figure 5b illustrates the variations in the measured lateral confining pressure with suction reduction. Once again, suction decreases induced growing pressures across all test series as soil expansive forces developed against the constant lateral confinement. Peak pressures often occurred within the initial high suction range above 50 kPa as the volume occupied by the adsorbed water layers increased the thicknesses of the diffused double layers.

Interestingly, lateral pressures exhibited the opposite behavior to vertical strains, with higher initial responses developing under elevated net stresses. For instance, maximum pressures of 44.7 kPa and 70.0 kPa were obtained at full saturation under zero net stress for OVS and OHS tests, yet these grew substantially larger under confinement. This confirms that confinement amplifies both vertical and lateral swelling capacities through stress–suction coupling effects. In addition, it should also be noted that the lateral pressures measured under zero net stress can be seen as pure swelling pressure, where the swelling pressure in the vertical direction (OHS-0) was 1.57 times that in the horizontal direction (OVS-0), also demonstrating an obvious swelling anisotropy as with swelling strain.

Notably, the OHS tests consistently produced higher lateral pressures than OVS runs across all suction–stress conditions, highlighting the greater development of expansive forces in the horizontal direction related to microstructural anisotropy.

In summary, the test results clearly demonstrated that the expansive soil exhibits anisotropic volumetric swelling strongly influenced by the stress state, moisture condition, and orientation of the layered mineral structure. These behaviors have significant implications for properly assessing and accommodating earth and swelling pressures in geostructure designs situated within expansive ground.

4. Developed Constitutive Model

4.1. Constitutive Model Expression

In a previous study, it was noted from the experimental results that the relationship between stress and strain could be considered an elastic process when the surcharge ranges from zero to the vertical swelling pressure measured under constant volume conditions [10]. The measured vertical swelling strain and lateral pressure under certain surcharges with saturated conditions were found to be quite close during the loading and unloading process [32]. Additionally, the earth pressure of unsaturated expansive soil would mobilize due to matric suction changes after rainfall. This single swelling process differs from the drying and wetting cyclical process, which can be regarded and assumed to be an elastic behavior. Therefore, to analyze the earth pressure of unsaturated expansive soil acting on a vertical retaining wall and investigate the mobilization of earth pressure distribution from the initial state to the saturation state, the interaction between the unsaturated expansive soil and the vertical retaining wall was simplified and regarded as a two-dimensional elastic problem.

Modifications were made to Fredlund's isotropic elastic model to characterize the anisotropic swelling behavior of expansive soil. The elastic modulus with respect to matric suction (H) was modified to consider two elastic moduli with respect to matric suction (H_v and H_h) in the vertical and horizontal directions, respectively. For simplicity, the elastic modulus with respect to net normal stress E was still considered isotropic. Therefore, the three-dimensional nonlinear elastic model can be further simplified as follows:

$$\begin{cases} d\varepsilon_h = \frac{d(\sigma_h - u_a)}{E} - \frac{\mu}{E} d(\sigma_h + \sigma_v - 2u_a) + \frac{ds}{H_h} \\ d\varepsilon_v = \frac{d(\sigma_v - u_a)}{E} - \frac{\mu}{E} d(\sigma_h + \sigma_h - 2u_a) + \frac{ds}{H_v} \end{cases}, \quad (1)$$

where ε_v and ε_h are the vertical and horizontal strain, respectively, in %; $(\sigma_v - u_a)$ and $(\sigma_h - u_a)$ are the vertical and horizontal net normal stress, respectively, in kPa; μ is the Poisson ratio; s is the matric suction, $s = u_a - u_w$, kPa; E is the elastic modulus with respect to net normal stress, in kPa; and H_v and H_h are the vertical and horizontal elastic moduli with respect to matric suction, respectively, in kPa.

4.2. Constitutive Parameters

In comparison with the original model, this modified constitutive model includes three elastic moduli, E, H_v, and H_h, all of which can be determined through modified unsaturated consolidation tests. In the modified unsaturated consolidation test, the specimen is subjected to constant net normal stress and gradually reduced matric suction, while always being subjected to lateral confinement, as shown in Figure 6.

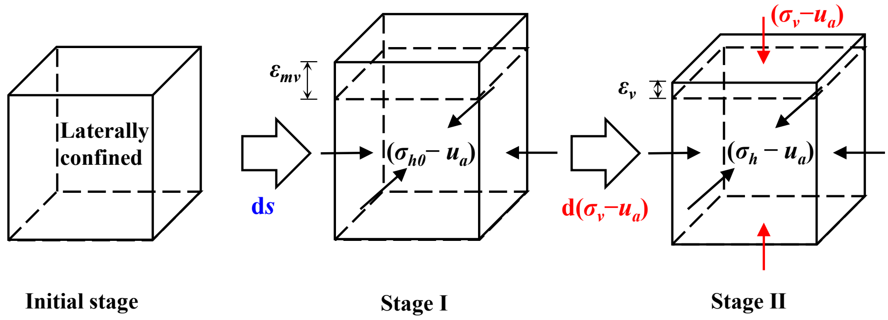

Figure 6. Stress state change of soil elements.

Assuming that the direction of the swelling is positive, Stage I demonstrates the stress state changes that occur in the soil elements of the specimen swelled under zero net normal stress from its initial matric suction to a specific matric suction level with lateral confinement. The lateral confining pressure without certain net normal stress is generated in the horizontal direction, and the maximum vertical swelling strain occurs in the vertical direction. The constitutive relationship at Stage I can be derived from Equation (1) and described by Equation (2):

$$\begin{cases} 0 = \frac{\mu-1}{E}\mathrm{d}(\sigma_{h0} - u_a) + \frac{\mathrm{d}s}{H_h} \\ \mathrm{d}\varepsilon_{mv} = \frac{2\mu}{E}\mathrm{d}(\sigma_{h0} - u_a) + \frac{\mathrm{d}s}{H_v} \end{cases}, \tag{2}$$

$$\mathrm{d}(\sigma_{h0} - u_a) = \frac{E}{(1-\mu)H_h}\mathrm{d}s, \tag{3}$$

$$\mathrm{d}\varepsilon_{mv} = \frac{2\mu}{1-\mu}\cdot\frac{\mathrm{d}s}{H_h} + \frac{\mathrm{d}s}{H_v}, \tag{4}$$

where σ_{h0} is the lateral confining pressure without certain net normal stress, and ε_{mv} is the maximum vertical swelling strain.

Equations (3) and (4) are derived by solving the previously derived equations to estimate the lateral confining pressure without certain net normal stress and the maximum vertical swelling strain at Stage I. The lateral confining pressure actually corresponds to the lateral swelling pressure associated with free swelling without certain net normal stress. In Stage II, the stress state changes occur in the soil elements of the specimen swelled under certain net normal stress from its initial matric suction to a specific matric suction level with lateral confinement. The lateral confining pressure under certain net normal stress is generated in the horizontal direction, and the vertical swelling strain under certain net normal stress occurs in the vertical direction. The constitutive relationship at Stage II can also be derived from Equation (1) and described by Equation (5):

$$\begin{cases} 0 = \frac{\mu-1}{E}\mathrm{d}(\sigma_h - u_a) + \frac{\mu}{E}\mathrm{d}(\sigma_v - u_a) + \frac{\mathrm{d}s}{H_h} \\ \mathrm{d}\varepsilon_v = -\frac{\mathrm{d}(\sigma_v - u_a)}{E} + \frac{2\mu}{E}\mathrm{d}(\sigma_h - u_a) + \frac{\mathrm{d}s}{H_v} \end{cases}, \tag{5}$$

$$\mathrm{d}(\sigma_h - u_a) = \frac{\mu}{1-\mu}\mathrm{d}(\sigma_v - u_a) + \frac{E}{(1-\mu)H_h}\mathrm{d}s, \tag{6}$$

$$\mathrm{d}\varepsilon_v = -\frac{(1-\mu-2\mu^2)\mathrm{d}(\sigma_v - u_a)}{(1-\mu)E} + \frac{2\mu}{1-\mu}\cdot\frac{\mathrm{d}s}{H_h} + \frac{\mathrm{d}s}{H_v}, \tag{7}$$

Comparing Equation (3) with Equation (6) and Equation (4) with Equation (7), it can be observed that these two pairs of equations have similar forms, with the difference being the presence of vertical net normal stress. In terms of elasticity, it can be understood that a vertical net normal stress ($\sigma_v - u_a$) is further loaded on the top of the specimen at Stage I. Under its influence, the vertical swelling strain decreases from the maximum value to the vertical swelling strain under surcharge, and the horizontal confining pressure generated in Stage I would further experience an increment and increase to ($\sigma_h - u_a$). During this period, the increment of matric suction is zero, namely ds = 0. The constitutive relationships from Stage I to Stage II can be described using Equation (8).

$$\begin{cases} 0 = \frac{\mu-1}{E}\mathrm{d}(\sigma_h - \sigma_{h0}) + \frac{\mu}{E}\mathrm{d}(\sigma_v - u_a) \\ \mathrm{d}(\varepsilon_v - \varepsilon_{mv}) = -\frac{\mathrm{d}(\sigma_v - u_a)}{E} + \frac{2\mu}{E}\mathrm{d}(\sigma_h - \sigma_{h0}) \end{cases}, \tag{8}$$

$$E = \frac{(1 - \mu - 2\mu^2)\mathrm{d}(\sigma_v - u_a)}{(1 - \mu)\mathrm{d}(\varepsilon_{mv} - \varepsilon_v)}, \tag{9}$$

where ($\varepsilon_v - \varepsilon_{mv}$) represents the reduction in vertical strain resulting from net normal stress.

Equation (9) is derived from Equation (8) to estimate the elastic modulus (E) with respect to the net normal stress. Once the net normal stress is loaded onto the specimen, it remains constant. Thus, the increment in net normal stress is zero, namely d($\sigma_v - u_a$) = 0. The first term on the right-hand side of Equation (7) equals zero, rendering this equation identical to Equation (4). This indicates that the vertical swelling strain of the unsaturated expansive soil is due to a moisture increment consisting of two parts. In addition to the vertical strain resulting from the change in matric suction itself, the lateral swelling strain would also occur if it were not laterally confined. The lateral confinement results in the representation of this part in the vertical direction. However, as mentioned in Section 2.2, the maximum radial strain of the oedometer ring is 0.032%. Therefore, the latter part could be extremely small compared to the previous part and can be ignored. Hence, the vertical swelling strain in OVS ($\varepsilon_{v,OVS}$) and the vertical swelling strain in OHS ($\varepsilon_{v,OHS}$) can be described as shown in Equation (10):

$$\begin{cases} \mathrm{d}\varepsilon_{v,OVS} = \frac{\mathrm{d}s}{H_v} \\ \mathrm{d}\varepsilon_{v,OHS} = \frac{\mathrm{d}s}{H_h} \end{cases}, \tag{10}$$

$$H_v = \frac{\mathrm{d}s}{\mathrm{d}\varepsilon_{v,OVS}}, \tag{11}$$

$$H_h = \frac{\mathrm{d}s}{\mathrm{d}\varepsilon_{v,OHS}}, \tag{12}$$

Equations (11) and (12) are derived from Equation (10) to estimate the vertical and horizontal elastic moduli (H_v and H_h) with respect to matric suction, respectively. For the determined unsaturated expansive soil, the change in vertical swelling strain is caused by the coupling effect of the net normal stress and matric suction. These three elastic parameters are all influenced by the changes in net normal stress and matric suction, demonstrating the nonlinear elastic behavior during wetting. However, Equation (9) would be invalid if the soil is inundated without vertical net normal stress, whereas the elastic modulus should be a property of the material itself. Although it may change under the influence of external factors (stress state and boundary conditions, etc.), it should always have an initial value. Equation (9) would need to be further modified based on the test results to estimate the E without the net normal stress.

Furthermore, Poisson's ratio is also essential for the constitutive model. Unsaturated expansive soil undergoes significant volume changes after saturation, leading to substantial changes in dry density. Soils with smaller dry densities are more likely to deform, and those with larger Poisson ratios are more susceptible to this deformation. However, recent standards do not provide methods for measuring the Poisson's ratio of unsaturated soils, nor do they specify the size of specimens and the testing conditions of stress and strain that are required for determining Poisson's ratio. In engineering practice, Poisson's ratio is often assumed to be a constant value. The suggested range of values for Poisson's ratio ranges from 0.2 (dry sand) to 0.5 (saturated clay tested under undrained conditions) [10,33].

5. Determination of the Elastic Parameters

5.1. Elastic Modulus with Respect to Net Normal Stress

The elastic modulus with respect to the net normal stress (E) characterizes the compressibility of the soil skeleton. It is required as a parameter within the proposed constitutive model relating stress–strain responses under changing net normal stresses or suction conditions.

As mentioned above, both the denominator and the numerator on the right-hand side of Equation (9) would become zero when no net normal stress is loaded, rendering it unable to estimate the elastic modulus E in this state. The elimination method can be carried out if there is a certain relationship between the denominator and the numerator. Figure 7 illustrates the variation curves of the denominator ($\varepsilon_v - \varepsilon_{mv}$) with respect to the numerator ($\sigma_v - u_a$).

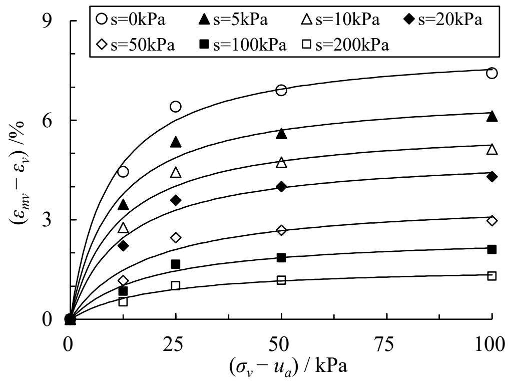

Figure 7. Variation curves of ($\varepsilon_{mv} - \varepsilon_v$) to ($\sigma_v - u_a$).

Figure 7 indicates that under the condition of constant matric suction, the increase in ($\varepsilon_{mv} - \varepsilon_v$) gradually increased with the increase in ($\sigma_v - u_a$), and the increment gradually decreased, tending to stabilize. The stress–strain relationship can be fitted in the form of a hyperbolic function, as shown in Equation (13). Table 3 shows that parameters a and b exhibited a strong correlation >0.95, validating the approach.

$$\varepsilon_{mvi} - \varepsilon_{vi} = \frac{a(\sigma_{vi} - u_a)}{1 + b(\sigma_{vi} - u_a)}, \tag{13}$$

where a and b are the fitting parameters.

Table 3. Fitting results of Equation (13).

Matric Suction (kPa)	a	b	R^2
200	0.0008	0.0524	0.9914
100	0.0014	0.0532	0.9908
50	0.0020	0.0545	0.9501
20	0.0039	0.0779	0.9829
10	0.0052	0.0882	0.9792
5	0.0067	0.0981	0.9814
0	0.0088	0.1070	0.9906

Substituting Equation (13) into Equation (9):

$$E = \frac{(1 - \mu - 2\mu^2)}{(1 - \mu)a/[1 + b(\sigma_{vi} - u_a)]}, \tag{14}$$

Comparing Equation (14) with Equation (9), Equation (14) is still valid in terms of estimating the elastic modulus E even in the absence of a vertical net normal stress. A series of elastic moduli E under different net normal stresses and matric suctions was estimated using Equation (14).

Figure 8 shows the variations in the calculated E values with changing net normal stress and suction states. Several trends were observed. E, with respect to net normal stress, decreased as matric suction decreased, showing a rapid reduction when the matric suction exceeded 20 kPa under a net normal stress of 50–100 kPa, while it gradually slowed down as the soil became increasingly saturated. With the decrease in net normal stress, the rapid reduction in E disappeared. Furthermore, under low net normal stress, matric suction had less impact on E than net normal stress. With an increase in net normal stress, the elastic modulus E under the same matric suction also increased, indicating that the influence of matric suction on E became much stronger. At the same matric suction level, a higher net normal stress led to a greater E. These results also highlight the fact that unsaturated expansive soil under low matric suction is more prone to deformation under external loads, and higher external loads enhance its resistance to deformation.

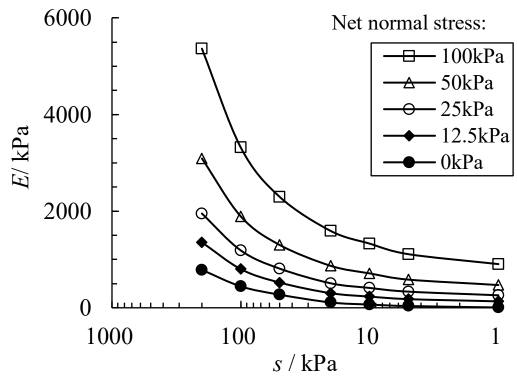

Figure 8. Variations in the elastic modulus E with different net normal stresses and suction states.

5.2. Elastic Modulus with Respect to Matric Suction

The elastic modulus with respect to matric suction reflects compressibility induced solely by suction changes independent of net stress effects. Both vertical (H_v) and horizontal (H_h) moduli were estimated to capture swelling anisotropy.

Equations (11) and (12) were applied to OVS and OHS test data to back-calculate H_v and H_h, respectively, from the slopes of the swelling strain–suction curves. Figure 9 presents the variations in the calculated H_v and H_h with suction reduction over different net normal stress levels.

Matric suction significantly influences the moduli of H_v and H_h. As matric suction decreases, both moduli monotonically decrease, with varying degrees of reduction for H_v and H_h. The moduli of H_v and H_h are relatively large when the matric suction is high, as the change in matric suction during this period does not significantly lead to changes in soil volume. Additionally, net normal stress also affects these moduli. Under the same matric suction, specimens subjected to higher net normal stresses have a larger elastic modulus than matric suction. This indicates that greater net normal stress leads to smaller swelling strain and larger swelling pressure. Consequently, the lateral swelling pressure, like the vertical swelling pressure, increases with net normal stress. The disparity between H_v and H_h can be considered a representation of swelling anisotropy on a macro scale.

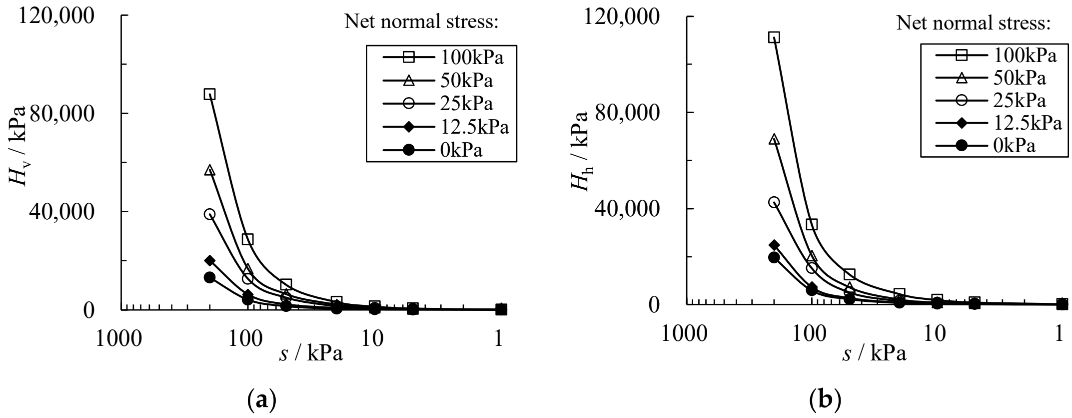

Figure 9. Variation curves of (**a**) H_v and (**b**) H_h with different matric suctions.

Notably, the moduli H_h exceeded H_v across all conditions, reflective of preferential horizontal restraint against intrinsically weaker lateral swelling. This separation quantifies the microstructural anisotropy manifestation in macroscopic stress–strain terms.

5.3. Prediction Method for Unsaturated Elastic Modulus

All of the elastic moduli calculated above are tangent moduli, regardless of whether they are E or H, while the calculation of lateral swelling pressure or lateral pressure is based on an incremental method, according to Equations (3) and (6). Therefore, in order to predict the unsaturated elastic modulus under certain net normal stress and matric suction states, the normalization of E by saturated E magnitude (E_{sat}) was subsequently performed, collapsing the data onto consistent power functions of normalized suction (Figure 10). The correlation coefficients exceeded 0.98, allowing predictive Equation (15) to estimate E_{unsat} from known saturated conditions. The values of the fitting parameters and their correlation coefficients are shown in Table 4. This simple expression captures modulus evolution, which is important for constitutive modeling.

$$E_{unsat} = E_{sat}\left[1 + \alpha\left(\frac{s}{s_0}\right)^{\beta}\right], \quad (15)$$

where α and β are fitting parameters, and s_0 is the initial matric suction of the soil.

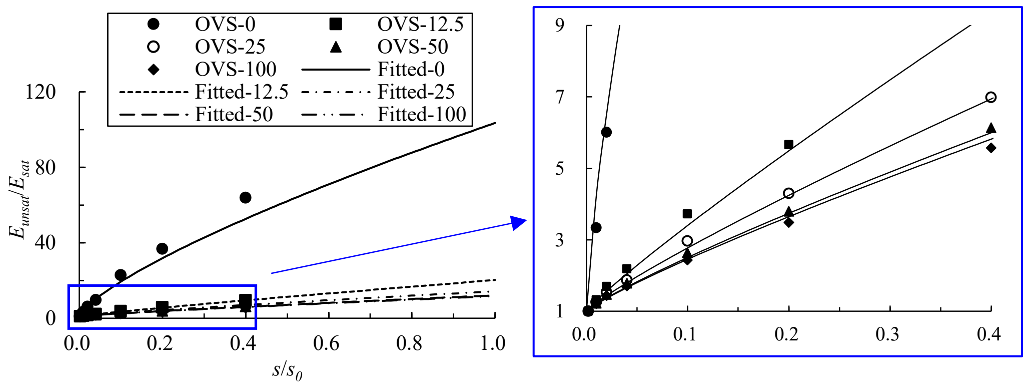

Figure 10. Normalization fitting curves of $E_{\mathrm{unsat}}/E_{\mathrm{sat}}$ to s/s_0.

The unsaturated modulus with respect to matric suction can be predicted in the same way. To normalize the data, Figure 11 plots H_{vunsat}/H_{vsat} and H_{hunsat}/H_{hsat} versus s/s_0, collapsing onto single best-fit power curves, as per Equation (16). The values of the fitting parameters and their correlation coefficients are shown in Table 5. Very strong correlations (more than 0.99) affirmed the predictability of this expression in terms of estimating the unsaturated elastic modulus H_{unsat} from the saturated conditions.

$$H_{unsat} = H_{sat}\left[1 + \lambda\left(\frac{s}{s_0}\right)^{\eta}\right], \tag{16}$$

where λ and η are the fitting parameters.

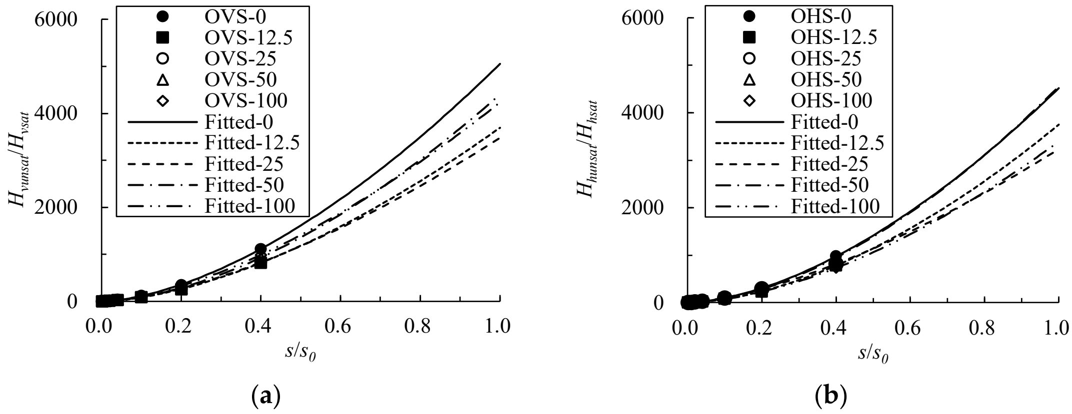

Figure 11. Normalization curves of (**a**) $H_{v\mathrm{unsat}}/H_{v\mathrm{sat}}$ to s/s_0 and (**b**) $H_{h\mathrm{unsat}}/H_{h\mathrm{sat}}$ to s/s_0.

Table 4. Fitting results between E_{unsat}/E_{sat} and s/s_0.

Net Normal Stress (kPa)	α	β	R^2
0	102.502	0.747	0.9851
12.5	19.224	0.904	0.9983
25	13.227	0.873	0.9986
50	11.047	0.866	0.9982
100	10.640	0.864	0.9960

Table 5. Fitting results between H_{unsat}/H_{sat} and s/s_0.

Net Normal Stress (kPa)	H_v			H_h		
	λ	η	R^2	λ	η	R^2
0	5050.221	1.648	0.9997	4518.053	1.673	0.9990
12.5	3694.508	1.646	0.9995	3750.679	1.710	0.9991
25	3479.687	1.567	0.9993	3232.893	1.502	0.9999
50	4396.977	1.694	0.9990	4553.960	1.712	0.9994
100	4229.299	1.585	0.9997	3393.036	1.676	0.9989

Moreover, it was observed that the datasets in Figure 11a,b were quite close to each other after normalization; hence, united fitting based on all of the datasets was further performed, and the fitting results show that the correlation coefficient is 0.9777, where the fitting parameter of λ is 4012.631 and η is 1.639, respectively. For convenient use in practical engineering applications, the united fitting method is recommended in the prediction of the unsaturated elastic modulus H_{unsat}.

The implementation of the proposed methods provides a practical means for determining the anisotropic expansive soil compressibility represented by H_{unsat}, which is a critical parameter within the constitutive framework for improved unsaturated expansive soil analyses.

6. Validation of Lateral Pressure Estimation

To evaluate the proposed techniques, lateral pressure estimations using the constitutive model were compared against experimental OVS and OHS test measurements. To further validate the anisotropy consideration, additional predictions were carried out treating

H_v and H_h as equal (isotropic assumption) rather than directionally dependent, namely Fredlund's nonlinear elastic model. Table 6 summarizes the parameter values obtained for input from the analyses presented in Sections 4 and 5.

Table 6. Summary of the calculating parameters used in the estimation.

Net Normal Stress (kPa)	E_{sat} (kPa)	H_{vsat} (kPa)	H_{hsat} (kPa)	H_{isosat} (kPa)	α	β	λ_v	η_v	λ_h	η_h
0	12	12	20	34	102.502	0.747	5050.221	1.648	4518.053	1.673
12.5	134	24	31	55	19.224	0.904	3694.508	1.646	3750.679	1.710
25	261	47	52	97	13.227	0.873	3479.687	1.567	3232.893	1.502
50	470	61	72	124	11.047	0.866	4396.977	1.694	4553.960	1.712
100	901	88	152	175	10.640	0.864	4229.299	1.585	3393.036	1.676

Note: H_{isosat}: the isotropic elastic modulus with respect to matric suction, $H_{isosat} = (1 + \mu)/(1 - \mu)\cdot ds/d\varepsilon_v$; λ_v and η_v: the fitting parameters for estimating H_{vunsat}; λ_h and η_h: the fitting parameters for estimating H_{hunsat}.

Elastically isotropic behavior was assumed within the stress range under consideration. Namely, the elastic moduli E in the vertical and horizontal directions were considered to be the same. All of the test series for the OVS and OHS tests provided lateral pressure datasets covering net normal stresses ranging from 0 to 100 kPa under staged suction reductions. Predictions were generated using Equations (3) and (6) with the appropriate elastic moduli at given stress states calculated using Equations (15) and (16).

Figure 12a overlays the estimated and measured lateral pressure variations across the decreasing matric suction path for each test. Remarkably close correlations were observed regarding the fact that the datasets are distributed near both sides of the 1:1 perfect prediction line, demonstrating the suitability of the proposed constitutive relationships and prediction methods. However, as shown in Figure 12b, it presents significantly poorer alignment that would increasingly underestimate the lateral pressure of expansive soil by 5.8–61.0%, which can be a disaster for engineers designing geo-infrastructure in expansive soil distributed areas. In addition, the deviations between the measured and predicted lateral pressures were found to be relatively large at higher stress states, whether using the proposed method or the isotropic model. This may be due to the fact that the expansive soil has already entered the plasticity state under such large stress and even yielded, where the elastic constitutive model can no longer characterize its stress–strain behavior. Therefore, this proposed model and method are suggested for use in designing light structures with lateral confinements at shallow depths.

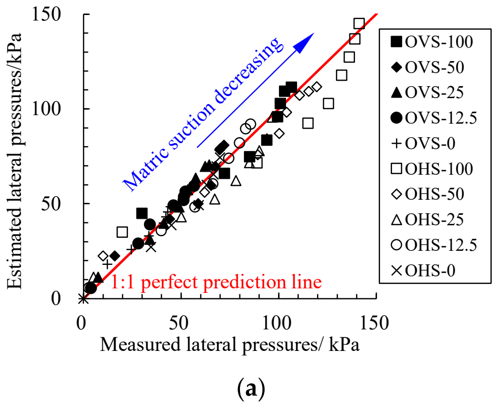

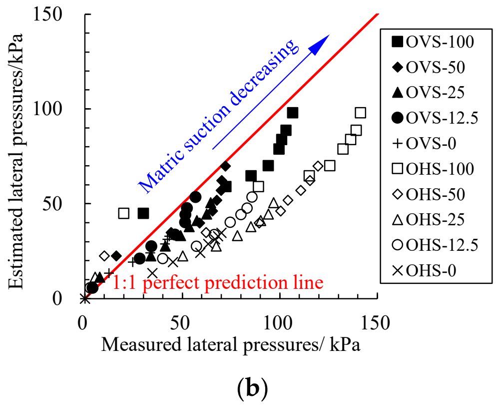

Figure 12. Comparison of the measured lateral pressure and the estimated lateral pressure by (**a**) the proposed method and (**b**) method without considering the anisotropic swelling behavior.

Five statistical indices were used to better evaluate the performance of the proposed method, including the correlation coefficient (R^2), refined Willmott index (RWI), mean arctangent absolute percentage error (MAAPE), root mean square error (RMSE), and mean absolute error (MAE). The model has larger R^2 and RWI, and smaller MAAPE, RMSE, and

MAE performed best [34]. The calculation results of those statistical indices are summarized in Table 7.

Table 7. Summary of the calculating statistical indices for all test series.

Test ID \ Indices	R^2		RWI		MAAPE (%)		RMSE		MAE	
	ANI	ISO	ANI	ISO	ANI	ISO	ANI	ISO	ANI	ISO
OVS-0	0.9899	0.9898	0.9239	0.7610	/	/	2.6975	8.6487	1.99	7.45
OVS-12.5	0.9966	0.9712	0.9118	0.7788	9.9	20.4	2.7427	7.7028	2.35	6.86
OVS-25	0.9858	0.9761	0.8513	0.6464	12.2	30.8	4.4998	14.1332	3.96	13.52
OVS-50	0.9410	0.8940	0.7553	0.6935	13.4	21.9	7.0124	12.9584	6.46	11.63
OVS-100	0.9362	0.9038	0.7978	0.6529	11.8	21.6	8.3822	17.4199	7.32	16.81
OHS-0	0.9816	0.9882	0.8873	0.5856	/	/	5.3509	30.2147	4.27	27.86
OHS-12.5	0.9828	0.9751	0.8898	0.6022	16.7	47.5	5.2837	29.7645	4.63	27.77
OHS-25	0.9746	0.9549	0.8055	0.5631	22.7	54.3	11.1098	41.2384	10.06	38.76
OHS-50	0.9850	0.9193	0.8520	0.5633	18.6	50.7	9.3792	46.3975	8.65	44.06
OHS-100	0.9464	0.8835	0.7976	0.5681	17.9	43.2	15.3981	46.4962	13.52	45.22

Note: ANI: estimation using the proposed method (anisotropic consideration); ISO: estimation using Fredlund's nonlinear elastic model (isotropic consideration).

As depicted in Table 7, it can be observed that the proposed method that considers the swelling anisotropy performed reasonably well in terms of determining the lateral pressure of expansive soil, and it has a superior predictive ability with higher R^2 and RWI values and lower MAAPE, RMSE, and MAE values compared to the isotropic model.

In conclusion, validation with high-quality test measurements affirmed the ability of the anisotropic constitutive model and estimation techniques to predict lateral pressures. Significant improvement over isotropic assumptions justifies the consideration of intrinsic anisotropy for more realistic expansive soil modeling and design. The results demonstrate the effectiveness of the proposed framework in capturing true stress–strain–suction behavior. With further refinement, the approach holds promise as a practical tool for facilitating the wider usage of expansive soils in geotechnical applications through proper earth pressure assessments.

7. Conclusions

This study conducted a comprehensive experimental investigation into the anisotropic swelling behavior of expansive soils and developed predictive methodologies to estimate earth pressures considering this inherent anisotropy. Based on the results and findings, the following conclusions were drawn:

(1) Modified oedometer testing quantified clear anisotropy in expansive soil, with a maximum vertical swelling strain 1.71 times that of the horizontal direction. The swelling pressures were also directionally dependent, and the vertical swelling pressure was 1.57 times that of the horizontal one.

(2) A nonlinear elastic constitutive model was proposed incorporating vertical and horizontal elastic moduli with respect to matric suction to characterize swelling anisotropy. Three key elastic moduli were determined from the test data.

(3) The elastic moduli decreased nonlinearly with saturation and increased under higher confinement, exhibiting strong dependence on stress state and suction. The differences between the horizontal and vertical moduli quantify the macroscale manifestation of microstructural anisotropy.

(4) Simple predictive equations were developed to estimate unsaturated elastic moduli from saturated conditions via normalization. Validation affirmed the use of a constitutive model and predictive techniques as useful engineering tools for earth pressure assessments that consider expansive anisotropy.

In conclusion, these findings provide an improved understanding of more realistic characterization and utilization of expansive soils in geotechnical applications by properly accounting for their inherent anisotropic behavior. However, deviations between the measured and predicted lateral pressures were found to be relatively large at higher stress states; this proposed model and method are suggested to be used in designing light structures with lateral confinement at shallow depths. In addition, studies based on in situ soils and soils from other locations are necessary to further validate the methodology presented in this paper, and studies on swelling in an angular direction with respect to the direction of compaction should also be carried out.

Author Contributions: Conceptualization, Z.L. and R.Z.; methodology, Z.L. and R.Z.; validation, Z.L., T.L. and C.H.; formal analysis, Z.L. and T.L.; data curation, Y.Z. and C.H.; investigation, Z.L. and Y.Z.; writing—original draft preparation, Z.L. and Y.Z.; writing—review and editing, Z.L., T.L. and R.Z.; supervision, R.Z.; funding acquisition, Z.L., R.Z. and T.L. All authors have read and agreed to the published version of the manuscript.

Funding: This research was funded by the National Natural Science Foundations of China, grant numbers 52308436 and 51978085; the Research and Development Program of China National Railway Group Co., Ltd., grant number K2023G033; the Open Fund of National Key Laboratory of Green and Long-Life Road Engineering in Extreme Environment (Changsha University of Science & Technology), grant number kfj230106.

Institutional Review Board Statement: Not applicable.

Informed Consent Statement: Not applicable.

Data Availability Statement: The raw data supporting the conclusions of this article will be made available by the authors on request.

Conflicts of Interest: Author Zhengnan Liu was employed by the company Hunan Communications Research Institute Co., Ltd. The remaining authors declare that the research was conducted in the absence of any commercial or financial relationships that could be construed as a potential conflict of interest.

References

1. Puppala, A.J. Performance evaluation of infrastructure on problematic expansive soils: Characterization challenges, innovative stabilization designs, and monitoring methods. *J. Geotech. Geoenviron. Eng.* **2021**, *2021*, 147. [CrossRef]
2. Yao, H.; She, J.; Lu, Z.; Luo, X.; Xian, S.; Fang, R.; Chen, Z. Inhibition effect of swelling characteristics of expansive soil using cohesive non-swelling soil layer under unidirectional seepage. *J. Rock Mech. Geotech. Eng.* **2020**, *12*, 188–196. [CrossRef]
3. Miao, L.; Wang, F.; Ye, W.; Jiang, M.; Li, J.; Shi, S. Combined method limiting shrinkage–swelling behaviours of expansive soils in Huai'an, China. *Environ. Geotech.* **2021**, *8*, 334–344. [CrossRef]
4. Zheng, J.; Zhang, R.; Yang, H. Highway subgrade construction in expansive soil areas. *J. Mater. Civ. Eng.* **2009**, *21*, 154–162. [CrossRef]
5. Zada, U.; Jamal, A.; Iqbal, M.; Eldin, S.M.; Almoshaogeh, M.; Bekkouche, S.R.; Almuaythir, S. Recent advances in expansive soil stabilization using admixtures: Current challenges and opportunities. *Case Stud. Constr. Mater.* **2023**, *18*, e01985. [CrossRef]
6. Zhang, J.; Ding, L.; Li, F.; Peng, J. Recycled aggregates from construction and demolition wastes as alternative filling materials for highway subgrades in China. *J. Clean. Prod.* **2020**, *255*, 120223. [CrossRef]
7. Sarker, D.; Apu, O.S.; Kumar, N. Sustainable lignin to enhance engineering properties of unsaturated expansive subgrade soils. *J. Mater. Civ. Eng.* **2023**, *35*, 04023259. [CrossRef]
8. Zhang, R.; Liu, Z.; Zheng, J.; Lei, G. Utilisation of expansive soils as highway embankment materials in humid environments. *Int. J. Pavement Eng.* **2022**, *23*, 2176–2190. [CrossRef]
9. Cui, X.; Li, X.; Du, Y.; Bao, Z.; Zhang, X.; Hao, J.; Hu, Y. Macro-micro numerical analysis of granular materials considering principal stress rotation based on DEM simulation of dynamic hollow cylinder test. *Constr. Build. Mater.* **2024**, *412*, 134818. [CrossRef]
10. Liu, Y.; Vanapalli, S.K. Influence of lateral swelling pressure on the geotechnical infrastructure in expansive soils. *J. Geotech. Geoenviron. Eng.* **2017**, *143*, 04017006. [CrossRef]
11. Oh, W.T.; Vanapalli, S.K. Modeling the stress versus settlement behavior of shallow foundations in unsaturated cohesive soils extending the modified total stress approach. *Soils Found.* **2018**, *58*, 382–397. [CrossRef]
12. Nelson, J.D.; Chao, K.C.; Overton, D.D.; Nelson, E.J. *Foundation Engineering for Expansive Soils*; John Wiley & Sons: Hoboken, NJ, USA, 2015.
13. Qi, S.; Vanapalli, S.K. Influence of swelling behavior on the stability of an infinite unsaturated expansive soil slope. *Comput. Geotech.* **2016**, *76*, 154–169. [CrossRef]
14. Tu, H.; Vanapalli, S.K. Prediction of the variation of swelling pressure and 1-D heave of expansive soils with respect to suction using the soil water retention curve as a tool. *Can. Geotech. J.* **2016**, *53*, 1213–1234. [CrossRef]

15. Fredlund, D.G.; Morgenstern, N.R. Constitutive relations for volume change in unsaturated soils. *Can. Geotech. J.* **1976**, *13*, 261–276. [CrossRef]
16. Adem, H.H.; Vanapalli, S.K. Prediction of the modulus of elasticity of compacted unsaturated expansive soils. *Int. J. Geotech. Eng.* **2015**, *9*, 163–175. [CrossRef]
17. Han, Z.; Vanapalli, S.K. State-of-the-Art: Prediction of resilient modulus of unsaturated subgrade soils. *Int. J. Geomech.* **2016**, *16*, 04015104. [CrossRef]
18. Avsar, E.; Ulusay, R.; Sonmez, H. Assessments of Swelling Anisotropy of Ankara clay. *Eng. Geol.* **2009**, *105*, 24–31. [CrossRef]
19. Jia, L.-Y.; Chen, Y.-G.; Ye, W.-M.; Cui, Y.-J. Effects of a Simulated Gap on Anisotropic Swelling Pressure of Compacted GMZ Bentonite. *Eng. Geol.* **2019**, *248*, 155–163. [CrossRef]
20. Saba, S.; Cui, Y.-J.; Barnichon, J.-D.; Tang, A.M. Infiltration column for studying the lateral swell behavior of expansive clay. *Geotech. Test. J.* **2016**, *39*, 407–414. [CrossRef]
21. Zhu, Y.; Ye, W.; Wang, Q.; Lu, Y.; Chen, Y. Anisotropic Volume Change Behaviour of Uniaxial Compacted GMZ Bentonite under Free Swelling Condition. *Eng. Geol.* **2020**, *278*, 105821. [CrossRef]
22. Sahin, H.; Slowey, N.C.; Lytton, R.L. Volume measurement of expansive soils and its application during the design of a retaining wall in Texas. *J. Mater. Civ. Eng.* **2018**, *30*, 04018114. [CrossRef]
23. Zou, W.-L.; Han, Z.; Vanapalli, S.K.; Zhang, J.-F.; Zhao, G.-T. Predicting volumetric behavior of compacted clays during compression. *Appl. Clay Sci.* **2018**, *156*, 116–125. [CrossRef]
24. Li, J.; Zhang, J.; Zhang, A.; Peng, J. Evaluation on deformation behavior of granular base material during repeated load triaxial testing by discrete-element method. *Int. J. Geomech.* **2022**, *22*, 04022210. [CrossRef]
25. Zhang, R.; Liu, Z.; Zheng, J.; Zhang, J. Experimental evaluation of lateral swelling pressure of expansive soil fill behind a retaining wall. *J. Mater. Civ. Eng.* **2020**, *32*, 04019360. [CrossRef]
26. Rawat, A.; Baille, W.; Tripathy, S. Swelling behavior of compacted bentonite-sand mixture during water infiltration. *Eng. Geol.* **2019**, *257*, 105–141. [CrossRef]
27. Abbas, M.F.; Elkady, T.Y.; Al-Shamrani, M.A. Evaluation of strain and stress states of a compacted highly expansive soil using a thin-walled oedometer. *Eng. Geol.* **2015**, *193*, 132–145. [CrossRef]
28. Liu, Z.; Zhang, R.; Liu, Z.; Zhang, Y. Experimental study on swelling behavior and its anisotropic evaluation of unsaturated expansive soil. *Adv. Mater. Sci. Eng.* **2021**, *2021*, 6937240. [CrossRef]
29. *ASTM D1557-12e1*; Standard Test Methods for Laboratory Compaction Characteristics of Soil Using Modified Effort (56,000 ft-lbf/Ft3 (2700 kN-m/m3)). American Society for Testing Materials: West Conshohocken, PA, USA, 2012.
30. CCCC (China Communications Construction Co., Ltd.); First Highway Consultants Co., Ltd. *JTG C20-2011 Code for Highway Engineering Geological Investigation*; China Communication Press: Beijing, China, 2011.
31. *ASTM D2435/D2435M-11*; Standard Test Method for One-Dimensional Consolidation Properties of Soils Using Incremental Loading. American Society for Testing Materials: West Conshohocken, PA, USA, 2011.
32. Zhang, R.; Zhang, B.; Zheng, J.; Liu, Z. Modified lateral confined swelling tests on expansive soils. *Chin. J. Geotech. Eng.* **2018**, *40*, 2223–2230. (In Chinese)
33. Kumar, S.; Cao, D.T.; Vahedifard, F. Poisson's ratio characteristic curve of unsaturated soils. *J. Geotech. Geoenviron. Eng.* **2021**, *147*, 04020149. [CrossRef]
34. Raja, M.N.A.; Shukla, S.K. Predicting the settlement of geosynthetic-reinforced soil foundations using evolutionary artificial intelligence technique. *Geotext. Geomembr.* **2021**, *49*, 1280–1293. [CrossRef]